Practical application of zone-folding concepts in tight-binding calculations

Timothy B. Boykin
Department of Electrical and Computer Engineering, The University of Alabama in Huntsville, Huntsville, Alabama 35899, USA

Gerhard Klimeck
Network for Computational Nanotechnology, School of Electrical and Computer Engineering, Purdue University, West Lafayette, Indiana 47907, USA

(Received 13 September 2004; revised manuscript received 9 December 2004; published 31 March 2005)

Modern supercell algorithms, such as those used in treating arrays of quantum dots or alloy calculations, are often founded upon local basis representations. Such local basis representations are numerically efficient, allow considerations of systems consisting of millions of atoms, and naturally map into carrier transport simulation algorithms. Even when treating a bulk material, algorithms formulated on a local basis generally cannot produce an $E(\mathbf{k})$ dispersion resembling that of a simple unit cell, due to zone folding. This paper provides an exact method for perfect supercells to unfold the zone folded $E(\mathbf{k})$ diagrams into a meaningful bulk dispersion relation. In addition, a modification to the algorithm for use with imperfect supercells is presented. With this method, questions such as algorithm verification, dispersions in nanowires, and dispersions in finite supercell heterostructures can be addressed.

DOI: 10.1103/PhysRevB.71.115215 PACS number(s): 71.20.−b, 73.21.Cd

I. INTRODUCTION

The band-structure calculation of atom clusters has been common practice in the computational exploration of modern material science.[1–3] Such calculations for materials are typically performed within a plane-wave basis in an infinitely periodic system. The resulting dispersion relationships in various crystal directions are critical for the evaluation of the material properties. In contrast to plane-wave basis set, one finds local basis sets theoretically and practically more convenient for the calculation of electronic transport in nanostructures[4] and more efficient with smaller computational requirements than corresponding pseudopotential methods for the calculation of electronic structure in multimillion-atom systems.[5,6] These advantages are fully utilized when finite size structures in finite environments are simulated. Such modern supercell algorithms have been employed in treating impurities,[7] quantum dots,[5] and alloys.[8]

Despite the preferred and primary use of the local basis sets for finite-size nanoelectronic structures, it is often instructive to also examine the system under some periodic boundary conditions, where periodicity may be considered in one, two, or three dimensions. Concrete examples for such applications of periodic boundary conditions are vertical transport in one-dimensional (1D) heterostructures with finite-size supercells [two-dimensional (2D) periodicity], calculation of zero-bias dispersion along a quantum wire with confinement in two dimensions (1D periodicity), and bulk band structure [three-dimensional (3D) periodicity]. Such a supercell treatment consisting of multiple small (i.e., primitive) cells results in multiple folding of the typical band structure $E(\mathbf{k})$ diagram into smaller Brillouin zones (see Fig. 1). Such multiple folding obscures the desired band-structure analysis. The fundamental question to be answered is whether a traditional $E(\mathbf{k})$ diagram can be reconstructed from the eigenvalues and eigenvectors of the small supercell Brillouin zone.

The answer to this question lies in the type of supercell being studied. If all of the small cells in the supercell are identical, then an exact reconstruction of a traditional $E(\mathbf{k})$ diagram is in principle possible. An efficient technique for an exact reconstruction would be of great utility in verifying supercell algorithms. That is, a correct supercell algorithm applied to a perfect crystal should give the same $E(\mathbf{k})$ dispersion, as does a conventional energy-band calculation.

If, on the other hand, the small cells comprising the supercell are not identical, perhaps having different atoms or different displacements of the atoms within the small cells, then only an approximate $E(\mathbf{k})$ relation is possible. Imperfect

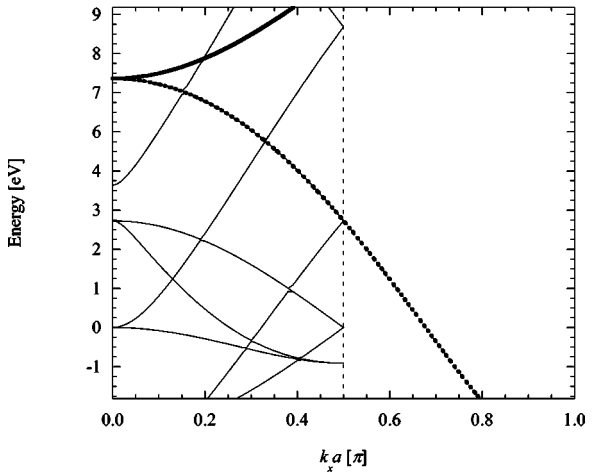

FIG. 1. Three of the bands along [100] for the simple cubic sp^3 system studied here (see text). Bulk bands for this system (i.e., those of the primitive cell, with the lattice parameter a) are plotted in bold; the solid line is double degenerate. Bands for a $2\times2\times2$ supercell along [100] are plotted with fine lines. Note that the bulk bands exactly overlap two of the supercell bands. The dashed line denotes the supercell Brillouin zone.

supercells such as this lack translational symmetry so that the wave vectors, $\mathbf{k}$, are no longer good quantum numbers, and, strictly speaking, the function $E(\mathbf{k})$ does not exist. If the disorder is not too great, then the best $E(\mathbf{k})$ that can be achieved is one belonging to a translationally symmetric system that mimics as closely as possible the actual system. The dispersion of this translationally symmetric system may then be said to approximate the properties of the actual system. Here the objective of zone unfolding is to reconstruct the best approximate $E(\mathbf{k})$ for the imperfect system.

The ideal unfolding method would be applicable to both perfect and imperfect supercells. For perfect supercells it would exactly reconstruct the small cell $E(\mathbf{k})$ relations. For imperfect supercells it would provide the best possible approximate reconstruction. Here we present an algorithm tailored for the empirical tight-binding method, which is exact and highly efficient for perfect supercells, and that can extract not only eigenenergies but in many cases the small cell eigenstates as well. For imperfect supercells, the great variety of systems that might be modeled (semiconductor alloys, arrays of nonidentical quantum dots, etc.) makes it far from clear at this point whether any single method will be best for all such cases. Nevertheless, the extension of the method for perfect supercells to imperfect ones presented shows much promise, and will likely be an integral part of approaches for the imperfect case. Section II discusses the exact algorithm for perfect supercells. Section III discusses its extension to the imperfect case and presents results for one example of a disordered system. Section IV presents the conclusions.

II. PERFECT SUPERCELLS

A useful unfolding method for perfect systems must take into account several complications common in supercell calculations. First, because most supercell calculations use an iterative method such as Lanczos,[9] even within a restricted range of energies only certain eigenvalues and eigenvectors are generally available. Hence an unfolding method must be able to deal with an incomplete spectrum efficiently, extracting as much information as possible about the bulk states. In addition, the supercell eigenvectors for a given eigenenergy are generally superpositions of bulk states at that energy, with the mixing generally being more severe for larger, more realistic, supercells. This distinction is important, because the bulk eigenenergies and eigenvectors are calculated as *functions* of the wave vector $\mathbf{k}$, making a hunt through the bulk spectrum for the desired eigenenergies an unattractive prospect. A useful unfolding algorithm must therefore yield both the corresponding bulk wave vectors and eigenvectors that contribute to a supercell state at a given energy.

The foregoing discussion suggests that an efficient verification method be built upon zone folding in its purest form, for that is precisely what happens in a calculation when only supercell (and not primitive cell) periodicity is imposed upon a bulk crystal. Zone folding is most often discussed in the context of semiconductor superlattices (e.g., $GaAs_mAlAs_n$),[10] and some of the more useful details of the pure form seem neglected in the literature. It is, however, these very details that lead to an efficient method for extraction of bulk eigenvectors from a supercell verification calculation.

The first step is to precisely determine the Brillouin zones of the two descriptions of the same crystal. Consider a bulk crystal with a primitive cell described by direct lattice vectors $\mathbf{a}_i$, $i=1,2,3$. In a conventional calculation a crystal of M_iN_i primitive cells along the direction $\mathbf{a}_i$, the wave vectors of the first Brillouin zone are

$$\mathbf{k}=\sum_{j=1}^{3}\frac{p_j}{M_jN_j}\mathbf{b}_j,\quad \mathbf{a}_i\cdot\mathbf{b}_j=2\pi\delta_{i,j}, \tag{1}$$

where the integers $p_j=q(M_jN_j)$ and the function q is defined by

$$q(Q)=\begin{cases}\dfrac{-(Q-2)}{2},\ldots,-1,0,1,\ldots\dfrac{Q}{2}, & Q \text{ even}\\ \dfrac{-(Q-1)}{2},\ldots,-1,0,1,\ldots\dfrac{(Q-1)}{2}, & Q \text{ odd.}\end{cases} \tag{2}$$

In a supercell calculation, on the other hand, the direct lattice vectors are now $\mathbf{A}_i=N_i\mathbf{a}_i$, $i=1,2,3$ for a supercell of N_i primitive cells along the direction $\mathbf{a}_i$. This same crystal then has M_i supercells along $\mathbf{A}_i$, and thus the supercell wave vectors $\mathbf{K}$, belonging to the first supercell Brillouin zone are

$$\mathbf{K}=\sum_{j=1}^{3}\frac{m_j}{M_j}\mathbf{B}_j=\sum_{j=1}^{3}\frac{m_j}{N_jM_j}\mathbf{b}_j,\quad \mathbf{B}_j=\frac{1}{N_j}\mathbf{b}_j, \tag{3}$$

where as usual the integers $m_j=q(M_j)$. Using Eqs. (1)–(3), it follows that for supercell reciprocal lattice vectors $\mathbf{G_n}=n_1\mathbf{B}_1+n_2\mathbf{B}_2+n_3\mathbf{B}_3, n_i$ integers, the equality

$$\mathbf{K}+\mathbf{G_n}=\sum_{j=1}^{3}\left(\frac{m_j}{M_j}\mathbf{B}_j+n_j\mathbf{B}_j\right)=\sum_{j=1}^{3}\frac{m_j+n_jM_j}{N_jM_j}\mathbf{b}_j=\mathbf{k} \tag{4}$$

holds, provided that the integers p_j, m_j, n_j, M_j satisfy

$$p_j=m_j+n_jM_j. \tag{5}$$

Analysis of this equation shows that for N_j odd (regardless of the parity of M_j), $\max(p_j)$ occurs for the pair $(m_j,n_j)=\{\max[q(M_j)],\max[q(N_j)]\}$, while in a like manner, $\min(p_j)$ occurs for the pair $(m_j,n_j)=\{\min[q(M_j)],\min[q(N_j)]\}$. For N_j, even the situation is somewhat different: $\max(p_j)$ occurs for $(m_j,n_j)=(0,N_j/2)$ but $\min(p_j)$ occurs for $(m_j,n_j)=(1,-N_j/2)$. In this case then, the limits on n_j are no longer prescribed by the function q, and this subtlety must be kept in mind when extracting bulk states from supercell eigenvectors.

The next step consists of comparing the wave function for a given energy in the conventional and supercell calculations. In the conventional calculation, the eigenstate of energy E_p with wave vector $\mathbf{k}$, is written

$$|\psi_{p,\mathbf{n}}(\mathbf{k})\rangle=\sum_{j=1}^{N_S}\sum_{\alpha,\mu}\sum_{l=1}^{N_C}\frac{e^{i\mathbf{K}\cdot\mathbf{R}_j}}{\sqrt{N_SN_C}}b_p^{(\alpha,\mu)}(\mathbf{K}+\mathbf{G_n})e^{i(\mathbf{K}+\mathbf{G_n})\cdot\boldsymbol{\rho}_l}\times|\alpha,\mu;\mathbf{R}_j+\boldsymbol{\rho}_l\rangle, \tag{6}$$

where the origin of the jth supercell is $\mathbf{R}_j$; the location of the

lth primitive cell relative to its supercell origin is $\boldsymbol{\rho}_l$; α the orbital type (s, p_x, etc.); μ the atom index within a primitive cell (for crystals with polyatomic bases); $N_C=N_1N_2N_3$ the number of primitive cells per supercell; and $N_S=M_1M_2M_3$ the number of supercells in the solid. The total number of (orbital, atom) pairs per primitive cell is denoted $N_{O,cell}$. In contrast, the supercell eigenstates are simultaneous eigenstates of energy and supercell wave vector, **K**, only,

$$|\Psi_p(\mathbf{K})\rangle = \sum_{j=1}^{N_S}\sum_{\alpha,\mu}\sum_{l=1}^{N_C}\frac{e^{i\mathbf{K}\cdot\mathbf{R}_j}}{\sqrt{N_S}}\beta_{l,p}^{(\alpha,\mu)}(\mathbf{K})|\alpha,\mu;\mathbf{R}_j+\boldsymbol{\rho}_l\rangle. \quad (7)$$

As mentioned above, the supercell eigenstates are generally superpositions of primitive-cell eigenstates. Using Eqs. (6) and (7),

$$|\Psi_p(\mathbf{K})\rangle = \sum_{j=1}^{N_C} a_{p,\mathbf{n}(j)}|\psi_{p,\mathbf{n}}(\mathbf{K}+\mathbf{G}_{\mathbf{n}(j)})\rangle, \quad (8)$$

where the notation $\mathbf{n}(j)$, $j=1,2,\ldots,N_C$ refers to the jth trio of integers **n** specifying a supercell reciprocal lattice vector $\mathbf{G}_\mathbf{n}$. A few comments regarding Eq. (8) are in order. First, often many of the coefficients $a_{p,\mathbf{n}}$ are zero since the primitive cell eigenstates of energy E_p coincide with only some wave vectors $\mathbf{K}+\mathbf{G}_\mathbf{n}$. Second, when there is a degeneracy in the primitive-cell spectrum (several states having the same energy, E_p, and wave vector, $\mathbf{K}+\mathbf{G}_\mathbf{n}$), the ket $|\psi_{p,\mathbf{n}}(\mathbf{K}+\mathbf{G}_\mathbf{n})\rangle$ appearing in Eq. (8) is the projection of the supercell eigenstate $|\Psi_p(\mathbf{K})\rangle$ onto the degenerate primitive cell subspace. (There is no unique basis for this subspace.)

Equation (8) leads directly to an efficient method for extraction of bulk states from the supercell states. Substituting Eqs. (6) and (7) into Eq. (8), projecting out the component for the ket $|\alpha,\mu;\mathbf{R}_j+\boldsymbol{\rho}_l\rangle$, and rearranging yields one of the N_C equations

$$e^{-i\mathbf{K}\cdot\boldsymbol{\rho}_l}\beta_{l,p}^{(\alpha,\mu)}(\mathbf{K}) = \frac{1}{\sqrt{N_C}}\sum_{j=1}^{N_C} a_{p,\mathbf{n}(j)}b_p^{(\alpha,\mu)}(\mathbf{K}+\mathbf{G}_{\mathbf{n}(j)})e^{i\mathbf{G}_{\mathbf{n}(j)}\cdot\boldsymbol{\rho}_l}. \quad (9)$$

In matrix form, these equations (one per primitive cell) read

$$\mathbf{B}_p^{(\alpha,\mu)}(\mathbf{K}) = \underline{\mathbf{U}}\cdot\mathbf{C}_p^{(\alpha,\mu)}(\mathbf{K}), \quad (10)$$

where

$$\mathbf{B}_p^{(\alpha,\mu)}(\mathbf{K}) = \begin{bmatrix} e^{-i\mathbf{K}\cdot\boldsymbol{\rho}_1}\beta_{1,p}^{(\alpha,\mu)}(\mathbf{K}) \\ \vdots \\ e^{-i\mathbf{K}\cdot\boldsymbol{\rho}_{N_C}}\beta_{N_C,p}^{(\alpha,\mu)}(\mathbf{K}) \end{bmatrix},$$

$$\mathbf{C}_p^{(\alpha,\mu)}(\mathbf{K}) = \begin{bmatrix} a_{p,\mathbf{n}(1)}b_p^{(\alpha,\mu)}(\mathbf{K}+\mathbf{G}_{\mathbf{n}(1)}) \\ \vdots \\ a_{p,\mathbf{n}(N_C)}b_p^{(\alpha,\mu)}(\mathbf{K}+\mathbf{G}_{\mathbf{n}(N_C)}) \end{bmatrix} \quad (11)$$

and the $N_C\times N_C$ unitary matrix $\underline{\mathbf{U}}$ is

$$\underline{\mathbf{U}} = \frac{1}{\sqrt{N_C}}\begin{bmatrix} e^{i\boldsymbol{\rho}_1\cdot\mathbf{G}_{\mathbf{n}(1)}} & e^{i\boldsymbol{\rho}_1\cdot\mathbf{G}_{\mathbf{n}(2)}} & \cdots & e^{i\boldsymbol{\rho}_1\cdot\mathbf{G}_{\mathbf{n}(N_C)}} \\ e^{i\boldsymbol{\rho}_2\cdot\mathbf{G}_{\mathbf{n}(1)}} & \ddots & \ddots & e^{i\boldsymbol{\rho}_2\cdot\mathbf{G}_{\mathbf{n}(N_C)}} \\ \vdots & \ddots & \ddots & \vdots \\ e^{i\boldsymbol{\rho}_{N_C}\cdot\mathbf{G}_{\mathbf{n}(1)}} & \cdots & \cdots & e^{i\boldsymbol{\rho}_{N_C}\cdot\mathbf{G}_{\mathbf{n}(N_C)}} \end{bmatrix}. \quad (12)$$

(The unitarity of the matrix $\underline{\mathbf{U}}$ follows directly from the fact that the $\boldsymbol{\rho}_j$ and $\mathbf{G}_\mathbf{n}$ are, respectively, direct lattice vectors and wave vectors of the first Brillouin zone for the primitive cell.[11])

To extract the bulk wave vectors and states, Eq. (10) is repeatedly solved (exploiting the unitarity of $\underline{\mathbf{U}}$, of course) for each (orbital, atom) combination (α,μ) and the results saved. Exploiting the normalization of the bulk eigenstates, the expansion coefficients $a_{p,\mathbf{n}}$, which give the contribution of each bulk state to a superlattice eigenstate, are obtained by summing over atoms and orbitals for a fixed energy, E_p, and supercell reciprocal lattice vector $\mathbf{G}_\mathbf{n}$

$$|a_{p,\mathbf{n}(j)}| = \sqrt{\sum_{\alpha,\mu}|[\mathbf{C}_p^{(\alpha,\mu)}]_j|^2},$$

$$[\mathbf{C}_p^{(\alpha,\mu)}]_j = a_{p,\mathbf{n}(j)}b_p^{(\alpha,\mu)}(\mathbf{K}+\mathbf{G}_{\mathbf{n}(j)}). \quad (13)$$

Since the overall phase of a bulk state is unimportant, the bulk coefficients follow immediately once the $a_{p,\mathbf{n}}$ have been determined

$$b_p^{(\alpha,\mu)}(\mathbf{K}+\mathbf{G}_{\mathbf{n}(j)}) = \frac{[\mathbf{C}_p^{(\alpha,\mu)}]_j}{|a_{p,\mathbf{n}(j)}|}. \quad (14)$$

Equations (13) and (14) are then repeatedly solved for each $\mathbf{G}_\mathbf{n}$ contributing to the superlattice eigenstate $|\Psi_p(\mathbf{K})\rangle$ to give the constituent bulk states. Carrying out the calculation of Eqs. (10)–(14) for all of the superlattice eigenstates yields

TABLE I. Bulk-state decompositions and contributions to superlattice states for the simple cubic $2\times2\times2$ supercell considered. The energy is −9.0002 eV and the superlattice wave vector is $\mathbf{K}=(0.01,0.01,0.01)(\pi/a)$, where a is the primitive cell lattice parameter; the phase of the s orbital for all states is set at $3\pi/2$. **k** is the bulk wave vector in units of (π/a). The bulk projections out of the supercell states yielded wave vectors $\mathbf{K}+\mathbf{G}_\mathbf{n}$, $\mathbf{G}_\mathbf{n}=\mathbf{n}(\pi/a)$, which, when shifted back into the bulk first Brillouin zone agree with the bulk **k**. The superlattice states are labeled $SL1$–$SL3$ and the figures in each of these columns are the contributions of the bulk states **k** to each, i.e., the $a_{p,\mathbf{n}}$ from Eqs. (8)–(11).

k	**n**	s	x	y	z	$SL1$	$SL2$	$SL3$
(−0.99,0.01,0.01)	(1,0,0)	$-i3.768\times10^{-2}$	-9.993×10^{-1}	3.229×10^{-4}	3.229×10^{-4}	3.854×10^{-1}	9.064×10^{-1}	1.732×10^{-1}
(0.01,−0.99,0.01)	(0,1,0)	$-i3.768\times10^{-2}$	3.229×10^{-4}	-9.993×10^{-1}	3.229×10^{-4}	8.263×10^{-1}	4.225×10^{-1}	3.724×10^{-1}
(0.01,0.01,−0.99)	(0,0,1)	$-i3.768\times10^{-2}$	3.229×10^{-4}	3.229×10^{-4}	-9.993×10^{-1}	4.107×10^{-1}	4.293×10^{-4}	9.118×10^{-1}

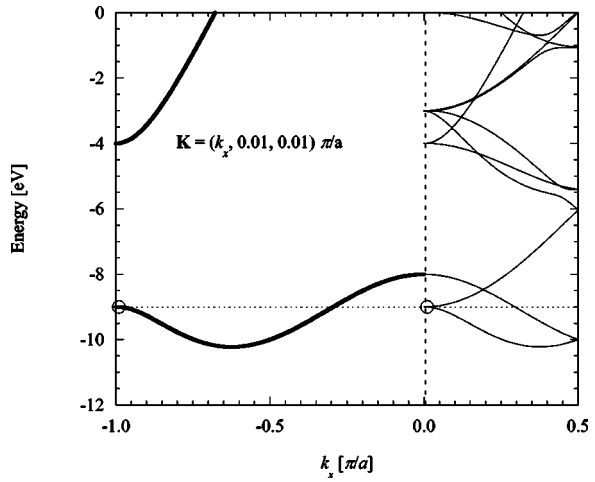

FIG. 2. Bulk bands (bold lines) and supercell bands (fine lines) for the $2\times2\times2$ supercell of Table I. The supercell state and one of the bulk states contributing to it are indicated with open circles. Note that the bulk bands are shown from the negative Brillouin zone face to zone center, while the supercell bands proceed from the zone center to their positive Brillouin zone face.

the maximum possible information about the bulk eigenstates.

Before examining specific examples, several comments on the efficient implementation of the method are in order. First, the matrix $\underline{\mathbf{U}}$ is independent of the superlattice wave vector $\mathbf{K}$, so it need be computed only once and reused for all $\mathbf{K}$ of interest. Since $\underline{\mathbf{U}}$ is unitary, computing its inverse to solve Eq. (10) is a trivial task. Second, solving Eq. (10) for each (orbital, atom) pair involves a computational burden of $N_{O,cell}$ matrix-vector multiplications of dimension N_C, costing $N_C^2 N_{O,cell}$ operations. This is more efficient than a straightforward single matrix-vector multiplication of dimension $N_C N_{O,cell}$, or $(N_C N_{O,cell})^2$ operations. (A special, sparse matrix-vector multiplication algorithm would be needed to limit the operation count to $N_C^2 N_{O,cell}$.) Finally, the same matrix $\underline{\mathbf{U}}$ can be employed even when some of the bulk wave vectors $\mathbf{K}+\mathbf{G_n}$ lie outside the first Brillouin zone of the primitive cell (i.e., when N_C is even), since Eqs. (2)–(5) can be used to shift these wave vectors back into the first zone.

A few numerical examples illustrate the method and the information obtainable from a supercell calculation. For ease of presentation, we choose a simple cubic lattice (lattice parameter a) with one atom per primitive cell, and a nearest-neighbor sp^3 tight-binding model. The Slater-Koster[12] parameters for our model are (in eV): $\varepsilon_s=-2.0$, $\varepsilon_p=5.0$, $V_{ss\sigma}=-1.0$, $V_{sp\sigma}=3.0$, $V_{pp\sigma}=4.0$, and $V_{pp\pi}=-1.5$.

TABLE II. Bulk states for comparison with projections from eigenstates of the $1\times2\times3$ supercell considered (Table III). The energy in 11.5 eV and the units for the wave vector $\mathbf{k}$ are (π/a), the same as in Table I. There are two degenerate bulk states ($B1$ and $B2$) at each wave vector; the s and z components of all of these states are zero.

$\mathbf{k}$	$B1$-x	$B1$-y	$B2$-x	$B2$-y
$(0,0,-2/3)$	0	1	1	0
$(0,0,2/3)$	0	1	1	0

As a first example (Table I), consider the supercell with $N_1=N_2=N_3=2$ having threefold degenerate states ($SL1$–$SL3$) at energy -9.0002 eV and supercell wave vector $\mathbf{K}=(0.01,0.01,0.01)(\pi/a)$. Each state is a superposition of the three bulk states $\mathbf{k}$ listed in the leftmost column of the table. The contributions of each of these bulk states to the supercell states are listed in the last three columns; Fig. 2 locates the first of these bulk states and the supercell state on $E(\mathbf{k})$ diagrams. The projection algorithm actually returned bulk wave vectors $\mathbf{K}+\mathbf{G_n}, \mathbf{G_n}=\mathbf{n}(\pi/a)$ for $\mathbf{n}$ in the second column of the table; when shifted back into the bulk first Brillouin zone these wave vectors matched the bulk $\mathbf{k}$. In all cases the same three bulk states were projected out of each of the three supercell states, and these projected bulk states agreed with those calculated directly from the bulk 4×4 Hamiltonian matrix. Even though they have the same energy, full recovery of the bulk states is possible because they have different $\mathbf{k}$. Note that when a supercell state is composed of multiple bulk states at different $\mathbf{k}$, the algorithm returns *all* of these constituent states in the decomposition of a single supercell state.

Consider next a case in which there are genuine degeneracies in the bulk spectrum and the limitations these place on the information obtainable from the supercell states (Tables II and III). The supercell has $N_1=1$, $N_2=2$, $N_3=3$ (6 primitive cells), and the superlattice wave vector is $\mathbf{K}=\mathbf{0}$. Table II shows that there are two bulk states at each of the wave vectors $\mathbf{k}_\pm=(0,0,\pm2/3)(\pi/a)$ for energy 11.5 eV. Table III shows that, as expected, each of the four supercell states at 11.5 eV and $\mathbf{K}=\mathbf{0}$ is composed of bulk states at both of these wave vectors. Figure 3 locates the supercell state at $\mathbf{K}=\mathbf{0}$ and the bulk state at $\mathbf{k}_+=(0,0,+2/3)(\pi/a)$ on the $E(\mathbf{k})$ diagrams. Note that the algorithm correctly determines the bulk wave vectors involved, but it no longer returns the same states as does the bulk calculation. Furthermore, the bulk states projected out of the supercell states are not orthogonal.

This lack of orthogonality can occur because there are bulk degeneracies at more than one bulk wave vector, $\mathbf{k}$.

TABLE III. Bulk states projected out of the supercell states at $\mathbf{K}=\mathbf{0}$, energy 11.5 eV for the $1\times2\times3$ supercell are considered (compare to the bulk states of Table II). The bulk wave vectors $\mathbf{k}$ in units of (π/a) are correctly projected out, and each of the four degenerate supercell states is an equal superposition of bulk states at $\mathbf{k}=(0,0,\pm2/3)(\pi/a)$, as indicated in the Weight column. The s and z components are zero in all cases and thus are not shown. While the superlattice states are orthonormal, the bulk states projected out of them are not (see text).

$\mathbf{k}$	Weight	$SL1$-x	$SL1$-y	$SL2$-x	$SL2$-y	$SL3$-x	$SL3$-y	$SL4$-x	$SL4$-y
$(0,0,-2/3)$	$1/\sqrt{2}$	0.4796	$0.8775e^{-i0.1702}$	0.9804	$0.1972e^{i3.0456}$	0.7504	$0.6610e^{-i2.3249}$	0.4958	$0.8684e^{-i4.988}$
$(0,0,2/3)$	$1/\sqrt{2}$	0.4796	$0.8775e^{i0.1702}$	0.9804	$0.1972e^{-i3.0456}$	0.7504	$0.6610e^{i2.3249}$	0.4958	$0.8684e^{i4.988}$

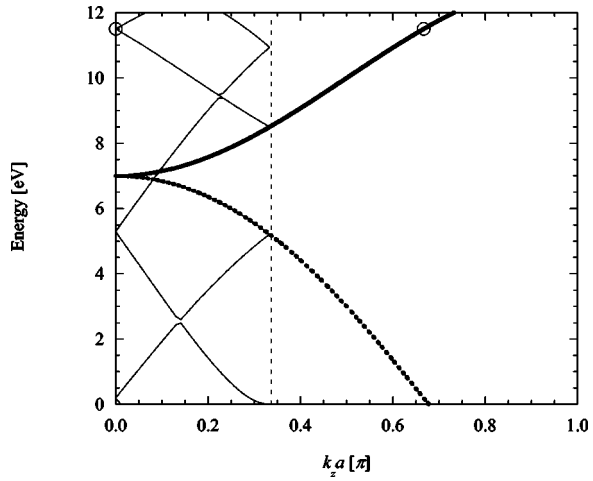

FIG. 3. Bulk bands (bold lines) and supercell bands (fine lines) for the $1\times2\times3$ supercell of Tables II and III. The supercell state at $\mathbf{K}=\mathbf{0}$ and one of the bulk states contributing to it are indicated with open circles.

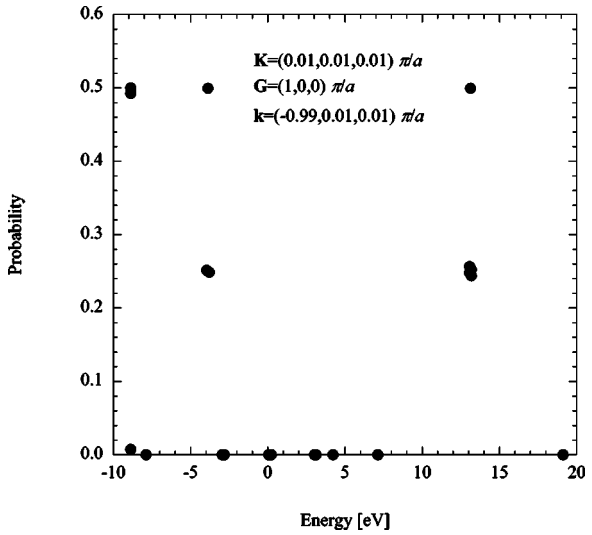

FIG. 4. Probability coefficients $|a_{p,\mathbf{n}}|^2$ for fixed $\mathbf{G}_{100}=(1,0,0)\pi/a$ from an imperfect $2\times2\times2$ supercell at $\mathbf{K}=(0.01,0.01,0.01)(\pi/a)$ (see text). There are 32 dots, one for each of the supercell states. Those energies at which the probability is greatest can be interpreted as being the band energies at this $\mathbf{k}=\mathbf{K}+\mathbf{G}_{100}$ for an averaged, translationally symmetric, Hamiltonian.

First, due to the bulk degeneracy at each of $\mathbf{k}_{\pm}$, the projections of the (orthogonal) supercell states onto the subspaces at $\mathbf{k}_{\pm}$ need not be identical. This differs from the case of Table I, where there is but one bulk state at the given energy per $\mathbf{k}$, and orthogonality is maintained via the weights $a_{p,\mathbf{n}}$. Second, the projections of the supercell states onto the $\mathbf{k}_{+}$ subspace need not be orthogonal since their (generally nonorthogonal) projections onto $\mathbf{k}_{-}$ subspace can compensate. Together with differing weights $a_{p,\mathbf{n}}$, this compensation keeps the four supercell states orthogonal. Of course, if all supercell states can be recovered, one can construct orthogonal bases for the degenerate bulk subspaces using the Gram-Schmidt procedure. Thus, in the presence of bulk degeneracies, the algorithm still recovers the bulk wave vectors; recovery of the bulk states themselves depends on the availability of supercell states.

III. IMPERFECT SUPERCELLS

In developing an extension of the projection method of Sec. II to the case of imperfect supercells, it is essential to always keep in mind that one can only speak of a meaningful band-structure $E(\mathbf{k})$ for an imperfect system so long as there exist translationally symmetric systems whose bands yield carrier dynamics approximating those of the actual, imperfect system. This is precisely the philosophy of conventional alloy calculations. For example, in calculating alloy bands with the virtual crystal approximation (VCA) as implemented in tight binding, one postulates a perfect crystal having tight-binding parameters given by an appropriate averaging of parameters from the constituent bulk materials. This postulated, translationally symmetric VCA Hamiltonian then has identical unit cells with "average" atoms in them, and its eigenstates are Bloch states of the form given in Eq. (6). Its bands are thus taken to approximate those of the actual system.

The extension of the method of Sec. II to imperfect supercells applies the philosophy of conventional alloy calculations in reverse. If physically meaningful, approximate band structures exist, then each must have its own translationally symmetric system, with identical small cells. These approximate perfect systems have, like the VCA Hamiltonian discussed above, Bloch states of the form, Eq. (6). The method of Sec. II may then be used to determine the contributions of each of these Bloch states to a given supercell state at small-cell wave vector $\mathbf{k}=\mathbf{K}+\mathbf{G}_{\mathbf{n}}$.

In an imperfect system, states at all available small-cell wave vectors $\mathbf{k}=\mathbf{K}+\mathbf{G}_{\mathbf{n}}$ will generally contribute to a given supercell state at $\mathbf{K}$, with the probabilities given by the $|a_{p,\mathbf{n}}|^2$. Note that this is unlike the case of a perfect supercell, where typically only some of the bulk states contribute to each supercell state (see Tables I–III). This fact leads to a method by which the supercell calculation *defines* the best average, translationally symmetric, approximating Hamiltonian. Roughly, the method proceeds as follows: the procedure of Sec. II is carried out on all of the supercell states obtained at a given $\mathbf{K}$. Then, for each of the N_C supercell reciprocal lattice vectors $\mathbf{G}_{\mathbf{n}}$ (each of which defines a small-cell wave vector $\mathbf{k}=\mathbf{K}+\mathbf{G}_{\mathbf{n}}$), a plot of the $|a_{p,\mathbf{n}}|^2$ is made with energy on the horizontal axis and probability on the vertical axis. The energies at which the probability is largest are taken to be the band energies of the translationally symmetric averaged Hamiltonian at small-cell wave vector $\mathbf{k}=\mathbf{K}+\mathbf{G}_{\mathbf{n}}$.

The algorithm outlined above will doubtless need further refinement. One open question is the exact nature of the averaging to be used to read off the peak energies. It is not clear to us at this point that one prescription will be best for all imperfect systems. For example, one type of averaging

might prove more appropriate for semiconductor alloys while another might work better for arrays of nonidentical quantum dots. Even with these important caveats in mind, very preliminary results show promise. Figure 4 is an example of such a calculation for an "alloy" supercell with $N_1=N_2=N_3=2$ for $\mathbf{K}=(0.01,0.01,0.01)(\pi/a)$. In this calculation the atoms in four of the small cells have their *s*- and *p*-onsite energies each increased by 0.25 eV. The $|a_{p,\mathbf{n}}|^2$ from the projections of each of the 32 supercell states onto small-cell Bloch states of $\mathbf{G}_{100}=(1,0,0)\pi/a$ are plotted as dots. Clear peaks are seen at roughly −9, −4, and 13 eV, and the point density is greatest around 13 eV (about twice that at the other peak energies). These energies can then be taken to be the approximate band energies at $\mathbf{k}=\mathbf{K}+\mathbf{G}_{100}$, with the greater density at about 13 eV indicating degenerate or nearly degenerate bands. Much far beyond the scope of this paper remains to be done to refine this approach, yet as Fig. 4 shows, it clearly has promise.

IV. CONCLUSIONS

We have demonstrated a computationally efficient means of verifying tight-binding supercell algorithms by extracting bulk wave vectors and eigenstates directly from the supercell states. Costly searches through the bulk spectrum are not required, and even explicit matrix inversions are unnecessary due to the unitarity of the matrix involved. The method shows promise for future extensions. Direct applications include arrays of quantum dots, and it may even have some utility in approximate treatment of semiconductor alloys.

ACKNOWLEDGMENTS

We acknowledge conversations with N. Vagidov. The work at Purdue was supported by the U. S. Army Research Office through the ARDA program and directly through ARDA, as well as by the National Science Foundation, Grant No. EEC-0228390.

[1] Alexander A. Demkov and Otto F. Sankey, Phys. Rev. B **48**, 2207 (1993).
[2] Xiang-Yang Liu, Wolfgang Windl, and M. P. Masquelier, Appl. Phys. Lett. **77**, 2018 (2000).
[3] K. C. Hass, L. C. Davis, and Alex Zunger, Phys. Rev. B **42**, 3757 (1990); T. Mattila, L.-W. Wang, and Alex Zunger, *ibid.* **59**, 15 270 (1999); P. R. C. Kent and Alex Zunger, *ibid.* **64**, 115208 (2001).
[4] Gerhard Klimeck, Roger K. Lake, R. Chris Bowen, William R. Frensley, and Ted Moise, Appl. Phys. Lett. **67**, 2539 (1995); Roger Lake, Gerhard Klimeck, R. Chris Bowen, and Dejan Jovanovic, J. Appl. Phys. **81**, 7845 (1997).
[5] Gerhard Klimeck, Fabiano Oyafuso, Timothy B. Boykin, R. Chris Bowen, and Paul von Allmen, Comput. Model. Eng. Sci. **3**, 601 (2002).
[6] A. Canning, L. W. Wang, A. Williamson, and A. Zunger, J. Comput. Phys. **160**, 29 (2000).
[7] J. G. Menchero and Timothy B. Boykin, Phys. Rev. B **59**, 8137 (1999).
[8] F. Oyafuso, G. Klimeck, R. C. Bowen, T. Boykin, and P. von Allmen, Phys. Status Solidi C **0**, 1149 (2003).
[9] G. H. Golub and C. F. van Loan, *Matrix Computations* (Johns Hopkins University Press, Baltimore, 1989), Chap. 9.
[10] L. Brey and C. Tejedor, Phys. Rev. B **35**, 9112 (1987).
[11] See, for example, N. W. Ashcroft and N. D. Mermin, *Solid State Physics* (Holt, Rinehart, and Winston, New York, 1976), Appendix F.
[12] J. C. Slater and G. F. Koster, Phys. Rev. **94**, 1498 (1954).